Journal of Drug Targeting

ISSN: 1061-186X (Print) 1029-2330 (Online) Journal homepage: http://www.tandfonline.com/loi/idrt20

Pendant HDAC Inhibitor SAHA Derivatized Polymer as a Novel Prodrug Micellar Carrier for Anticancer Drugs

Jieni Xu, Jingjing Sun, Pengcheng Wang, Xiaochao Ma & Song Li

To cite this article: Jieni Xu, Jingjing Sun, Pengcheng Wang, Xiaochao Ma & Song Li (2017): Pendant HDAC Inhibitor SAHA Derivatized Polymer as a Novel Prodrug Micellar Carrier for Anticancer Drugs, Journal of Drug Targeting, DOI: 10.1080/1061186X.2017.1419355

To link to this article: https://doi.org/10.1080/1061186X.2017.1419355

Accepted author version posted online: 18 Dec 2017.

Pendant HDAC Inhibitor SAHA Derivatized Polymer as a Novel Prodrug Micellar Carrier for Anticancer Drugs

Jieni Xu[a,b,c], Jingjing Sun[a,b,c], Pengcheng Wang[a,b], Xiaochao Ma[a,b] and Song Li[a,b,c,*]

[a]Center for Pharmacogenetics, University of Pittsburgh, Pittsburgh, PA 15261, USA

[b]Department of Pharmaceutical Sciences, School of Pharmacy, University of Pittsburgh, Pittsburgh, PA 15261, USA

[c]University of Pittsburgh Cancer Institute, University of Pittsburgh, Pittsburgh, PA 15261, USA

Corresponding Author

*Song Li, M.D., Ph.D.; Tel, 412-383-7976; Fax, 412-648-1664; Email: sol4@pitt.edu; Center for Pharmacogenetics, Department of Pharmaceutical Sciences, University of Pittsburgh School of Pharmacy, 313 Salk Pavilion, Pittsburgh, PA 15261.

Key Words: Vorinostat, Doxorubicin, Co-delivery, Prodrug micelles

Abstract:

Suberoylanilide hydroxamic acid (SAHA), a histone deacetylase inhibitor (HDACI) approved by FDA for the treatment of cutaneous T cell lymphoma, is a promising anticancer drug for various cancers with a unique mode of action. However, it demonstrates limited clinical benefits in solid tumors as a single drug. In order to achieve enhanced and synergistic co-delivery of SAHA and Doxorubicin (DOX), a cleavable SAHA-based prodrug polymer (POEG-*b*-PSAHA), consisting of hydrophilic poly(oligo(ethylene glycol) methacrylate) (POEG) blocks and hydrophobic SAHA segments, has been developed. POEG-*b*-PSAHA prodrug polymer was able to form spherical micelles with a diameter around 60 nm, and well retained the pharmacological activity of SAHA in either inhibiting the proliferation of tumor cells or inducing histone acetylation. DOX formulated in POEG-*b*-PSAHA-based micelles showed a sustained release profile. DOX-loaded POEG-*b*-PSAHA exhibited more potent cytotoxicity towards tumor cells than free DOX and DOX loaded in a pharmacologically "inert" nanocarrier, POEG-*b*-POM. Consistently, DOX/POEG-*b*-PSAHA formulation resulted in an improved therapeutic effect *in vivo* compared to free DOX, Doxil, or DOX formulated in POEG-*b*-POM micelles. These results suggest that SAHA-based prodrug micelles may serve as a dual functional carrier for combination strategies in epigenetic-oriented anticancer therapy.

1. Introduction:

Cancer development and progression is not only confined to genetic changes, but also involves epigenetic changes, leading to alterations in gene expression and cell phenotypes. Epigenetics is concerned with the heritable phenotypes based on changes in chromosome, as opposed to genetics, whose realm is on the basis of alterations in the primary DNA sequence (Avendaño and Menéndez, 2015, Berger et al., 2009). Alterations in the structure and modification status of chromatin represent powerful regulatory mechanisms for gene expression and genome stability (Avendaño and Menéndez, 2015). The major epigenetic modifications in mammals, and particularly in humans, are DNA methylation and post-translational histone modifications (acetylation, methylation, phosphorylation etc.) (Gibney and Nolan, 2010). In the context of histone modifications, the acetylation status of histones plays a crucial role in regulating gene expression by affecting the accessibility of DNA around them (Kouzarides, 2007). Acetylation levels are controlled by the balance of two enzymes families: histone acetyltransferase (HAT) and histone deacetylase (HDAC). HAT facilitates the acetylation of lysine in histone tails, which is associated with a more relaxed chromatin state, opening up access for transcription factors and polymerases, and therefore gene-transcription activation. In contrast, HDACs deacetylate the lysine residues thereby promoting a more condensed chromatin state and hence leading to transcriptional gene silencing (Grunstein, 1997, Gregory et al., 2001). Specially, the removal of the acetyl groups by HDACs also exposes the protonated amino groups of lysine units of histones, thereby increasing ionic interactions between the positively charged histones and negatively charged phosphate backbone of DNA, which yields a more compact chromatin structure and represses gene transcription by limiting the accessibility of the transcription machinery (Gregory et al., 2001).

A growing body of evidence indicates that the silence of tumor suppressor genes caused by HDAC overexpression could be a common phenomenon in tumor onset and progression (Zhu et al., 2004, Halkidou et al., 2004, Song et al., 2005). Therefore, there is growing interest in the development of HDAC inhibitors (HDACi) as anticancer agents and a large number of studies demonstrated the potential of HDACi in different cancer cell lines and in animal models of tumors (Marks et al., 2001, Johnstone, 2002, Falkenberg and Johnstone, 2014). The oral drug Vorinostat, also known as SAHA (from suberoylanilide hydroxamic acid) was the first HDAC inhibitor approved by the U.S. FDA in 2006 for the treatment of cutaneous T cell lymphoma in patients who have progressive, persistent or recurrent disease or following failure of two systemic therapies. It was also approved for multiple myeloma with slight advantage over Velcade®. SAHA is a pan-HDAC inhibitor and inhibits both classes I and II enzymes, but does not inhibit HDACs belonging to class III (Marks, 2007, Marks et al., 2001). SAHA acts as a micromolar inhibitor of HDACs by chelating the zinc atoms in HDAC catalytic sites via its hydroxamic end, with the phenyl ring protruding out of the binding pocket and lying on the hydrophobic surface of HDAC (Marks and Breslow, 2007). SAHA blocks the proliferation of cultured tumor cells and suppresses tumor growth in a variety of tumor models including prostate cancer (Butler et al., 2000), breast cancer (Cohen et al., 1999), leukemia (He et al., 2001), glioma (Eyupoglu et al., 2005) and lung cancer (Desai et al., 2003) with little or no toxicity.

Although SAHA has significant anticancer activity as a monotherapy in hematological malignancies, it demonstrates limited clinical benefit for patients with solid tumors, prompting the investigation of novel combination treatments with existing neoplastic interventions (Thurn et al., 2011). Besides, the acceptable toxicity profile of SAHA permits a broad integration into currently approved chemotherapy regimens (Munster et al., 2009,

Marchion et al., 2005b, Marchion et al., 2005a). Based on a mechanistic rationale, SAHA has been shown to be additive or synergistic with a wide array of anticancer drugs, including conventional chemotherapeutics (doxorubicin, paclitaxel, cisplatin, gemcitabine, 5-fluorouracil and etoposide) (Arnold et al., 2007, Dowdy et al., 2006, Rikiishi et al., 2007, Kim et al., 2003), targeted agents (imatinib, bevacizumab and trastuzumab) (Nimmanapalli et al., 2003, Fuino et al., 2003) and transcriptional modulators (all-trans retinoic acid and the demethylating agent 5-aza-2′-deoxycytidine) (Cameron et al., 1999). One of the most significant combinations is with DNA damage-inducing therapies, which occurs, in part, through a SAHA-mediated increase in chromatin accessibility and downregulation of DNA repair (Thurn et al., 2011). Doxorubicin induces DNA strand breaks by binding to DNA, stabilizing the Topo II-DNA complex, and inhibiting the re-ligation of DNA strands during replication (Thorn et al., 2011). SAHA potentiates DOX-induced Topo II-mediated DNA damage, growth inhibition and cell death through the chromatin decondensation, facilitating the access of topo II inhibitors to their DNA substrate (Marchion et al., 2005b, Marchion et al., 2005a). Moreover, the synergy is further intensified by the effect of SAHA on the expression, regulation and activation of a variety of DNA repair and DNA damage response genes, like Ku70 (Chen et al., 2007).

Although the combination of SAHA and other anticancer agents helps, to some extent, achieve better treatment of cancer, the triumph of simple physical mixture of multiple drugs is largely hindered as a result of poor solubility, minimal distribution to tumor tissue, and suboptimal dose ratio (Parhi et al., 2012). Carrier-mediated combination therapy could offer some advantages to overcome the above challenges, including improved solubility and bioavailability of each drug, increased accumulation at tumor sites through EPR effect, synchronized and controlled pharmacokinetics of each drug and ratiometric dosing, that is,

the ability to tailor the relative ratios of each agent based on its pharmacological disposition (Lee and Nan, 2012).

Among the commonly used drug delivery systems, polymers with diverse structures have been widely selected as the nanocarriers for hydrophobic anticancer drugs, including SAHA, DOX, and others. Several nanoscopic formulations of SAHA have been developed for parenteral administrations to improve the solubility and overall disposition profile. For example, PEG-b-PLA block copolymer-based micelles have been employed as a carrier to encapsulate SAHA, and it was found that SAHA loaded in micelles provided sustained exposure and improved pharmacokinetics characterized by a significant increase in serum $t_{1/2}$, AUC and mean residence time (Mohamed et al., 2012). However, the use of a large amount of pharmacologically inert carriers may not only add to the cost but also imposes safety issue (Croy and Kwon, 2006). Prodrug polymer nanocarriers represent an effective strategy to reduce the amount of inert materials. More importantly, amphiphilic prodrug polymers self-assemble in aqueous solution and serve as dual-functional carriers to achieve the additive or synergistic effect with co-delivered anticancer drugs.

In this study, we designed and synthesized SAHA-based prodrug polymer, denoted as POEG-*b*-PSAHA. These amphiphilic polymers could self-assemble into prodrug micelles and serve as nanocarriers for DOX delivery. The size and structure of POEG-*b*-PSAHA were characterized. Moreover, the *in vitro* pharmacological activity of POEG-*b*-PSAHA prodrug micelles was examined and compared with free SAHA. Finally, the antitumor activity of DOX-loaded POEG-*b*-PSAHA micelles was investigated in a syngeneic breast cancer model.

2. Methods

2.1 Materials

Aniline, N,N′-dicyclohexylcarbodiimide, 4-(dimethylamino)pyridine, hydroxylamine hydrochloride, 1-hydroxybenzotriazole hydrate, potassium carbonate, potassium hydroxide, vinylbenzyl chloride, 4-cyano-4-[(dodecylsulfanylthiocarbonyl)sulfanyl]pentanoic acid, oligo(ethylene glycol) methacrylate OEGMA (average Mn = 500), 2,2-Azobis(isobutyronitrile) (AIBN), trypsin-EDTA solution, 3-(4,5-dimethylthiazol-2-yl)-2,5-diphenyl tetrazolium bromide (MTT) and Dulbecco's Modified Eagle's Medium (DMEM) were all purchased from Sigma-Aldrich (MO, USA). AIBN was purified by recrystallization in anhydrous ethanol. Monomethyl suberate was purchased from TCI (OR, USA). DOX.HCl was purchased from LC Laboratories (MA, USA). Fetal bovine serum (FBS) and penicillin-streptomycin solution were purchased from Invitrogen (NY, USA.). Cell culture and animals were similarly handled as described before (Zhang et al., 2014b).

2.2 Methods

2.2.1 Synthesis of SAHA-monomer

SAHA was synthesized following a published method (Chung et al., 2013).

Vinylbenzyl chloride (1.0 g, 6.6 mmol), succinic acid (7.7 g, 66.0 mmol, 10 equiv) and K_2CO_3 (4.5 g, 32.8 mmol, 5 equiv) were dissolved in 30 mL DMF and immersed into an oil bath at 90 °C. After 4 h, the mixture was filtered through cottons to remove excess amount of salt. The reaction was quenched by addition of excess amount of pure water and centrifuged to remove DMF. The precipitate was dissolved in DCM, and the crude product was purified by column chromatography on silica gel eluted with ethanol/DCM (v/v, 1: 9) to give the Compound 1 (1.4 mg, 91%).

For the synthesis of SAHA-monomer, CDI (69 mg, 0.43 mmol, 1.2 equiv) was added in portions to a stirred solution of Compound 1 (100 mg, 0.43 mmol, 1.2 equiv) in DCM. After stirring for 10 min, the reaction mixture turned into light yellow color. TLC showed that the intermediate was formed, and then SAHA (94 mg, 0.36 mmol) was added to the mixture in portions. After 2 h, the reaction was complete as confirmed by TLC, and the reaction was quenched by the addition of the saturated sodium bicarbonate. The aqueous layer was extracted with DCM, washed with brine, and dried over $MgSO_4$. The crude product was chromatographed on silica gel (ethyl acetate/hexane =2:1) to give SAHA monomer (125 mg, 69%).

2.2.2 Synthesis of POEG macroCTA

POEG macroCTA was synthesized and purified following a published literature (Sun et al., 2016).

2.2.3 Synthesis of POEG-*b*-PSAHA

POEG macroCTA (150 mg, 0.02 mmol), SAHA-monomer (125 mg, 0.26 mmol, 13 equiv), AIBN (1 mg, 0.0061 mmol, 0.3 equiv) and 2 mL dried 1, 4-Dioxane were added into An Schlenk tube and deoxygenated by free-pump-thawing for three times. The mixture was then protected under N_2 and immersed into an oil bath at 90 °C. After 24 h, the reaction was quenched by immersing the tube into liquid nitrogen. The mixture was purified through three cycles of dissolution/precipitation in DCM/hexane, and dried in vacuum to afford POEG-*b*-PSAHA (260mg, 96%).

2.2.4 Preparation and characterization of DOX-loaded POEG-*b*-PSAHA micelles

The blank or DOX-loaded POEG-*b*-PSAHA micelles were prepared through the film hydration method. First, DOX.HCl was neutralized with 3 equivalents of triethylamine in a mixture of DCM/methanol (1:1, v/v). DOX (5 mg/mL) was then mixed with POEG-*b*-PSAHA (50 mg/mL in DCM) at various carrier/drug weight ratios. After removing the solvent by nitrogen flow, the thin film was formed, which was further dried under vacuum for 2 h to remove any trace of remaining solvent. Then the thin film was hydrated with PBS followed by vortexing. The blank micelles were similarly prepared. The average diameter and the size distribution of micelles were examined via a Zetasizer (DLS). The morphology of blank or DOX-loaded POEG-*b*-PSAHA micelles was observed using transmission electron microscopy (TEM).

The drug loading efficiency of DOX was examined by Waters Alliance 2695 Separations Module combined with Waters 2475 Fluorescence Detector (excitation, 490 nm; emission, 590 nm; gain, 3; sensitivity (FUFS), 10 000) and high performance liquid chromatography (HPLC) respectively as described in previous publications (Zhang et al., 2014a). Drug loading capacity (DLC) and drug loading efficiency (DLE) were calculated according to the following equation: DLC %= [weight of drug loaded/(weight of polymer used + weight of drug used)]×100%, DLE %= (weight of loaded drug/weight of input drug)×100 %. The colloidal stability of drug-loaded micelles with various carrier/drug molar ratios at 4°C was evaluated by following the changes in sizes of the particles or visible precipitates every hour in the first 12 h and daily after 12 h following sample preparation.

The CMC of POEG-*b*-PSAHA was measured by fluorescence spectrometry using nile red as a fluorescence probe. Briefly, thirty microliters of nile red (0.05 mg/mL in DCM) were added

to each tube and the solvent was removed by nitrogen flow. POEG-*b*-PSAHA micelles ranging from 6.1×10^{-5} to 5×10^{-1} mg/mL were prepared with serial dilution as described above and then added into the tubes with nile red. The final concentration of nile red was kept at 6.0×10^{-7} M. The micelles were vortexed and kept overnight at room temperature to reach the equilibrium of solubilization. The samples were excited at an excitation wavelength of 550 nm and fluorescence intensities were recorded at an emission spectrum from 600 to 700 nm. The peak intensities at 647 nm were plotted versus polymer concentrations. The CMC value was calculated as the cross-point where a sharp increase in fluorescence intensity was observed.

The *in vitro* release of DOX from DOX-loaded POEG-*b*-PSAHA micelles was examined using a dialysis method. Briefly, two hundred and fifty microliters of DOX/POEG-*b*-PSAHA micelles or free DOX·HCl (0.5 mg DOX/mL) were transferred to clamped dialysis bags (MWCO 3500 Da) in triplicate and incubated in 50 mL PBS as release medium, with gentle shaking at 100 rpm at 37 °C. One milliliter of medium was withdraw and same volume of fresh medium was supplemented at 10 min, 0.5, 1, 2, 4, 6, 8, 10, 12, 24, 48 and 72 h. DOX release from micelles was measured by fluorescence spectrometry at the excitation wavelength of 480 nm and emission wavelength of 590 nm by Synergy H1 Hybrid Multi-Mode Microplate Reader (Winooski, VT).

2.2.5 *In vitro* cytotoxicity assay

Cytotoxicity assay was performed with 4T1.2 mouse breast cancer cells, MCF-7 human breast cancer cells, and HCT-116 human colon cancer cells. 4T1.2 (1×10^3 cells/well), MCF-7 (5×10^3 cells/well), or HCT-116 (2×10^3 cells/well) cells were seeded in 96-well plates followed by 24 h of incubation in DMEM with 10% FBS and 1% streptomycin/penicillin. To evaluate the combinational effect of SAHA with other anticancer drugs, various

concentrations of free SAHA, free DOX·HCl, or the combination of both were added in triplicate to cells and incubated for 48 h. To study the cytotoxicity of blank POEG-*b*-PSAHA micelles, cells were challenged with various concentrations of POEG-*b*-PSAHA micelles or free SAHA (in DMSO) at equivalent SAHA concentrations for 48 h. The cytotoxicity of DOX-loaded POEG-*b*-PSAHA micelles was also examined, in comparison to DOX.HCl and DOX loaded in a biologically inert polymer POEG-*b*-POM. Cells were treated with different DOX formulations of varied concentrations. Blank POEG-*b*-PSAHA or POEG-*b*-POM at concentrations equivalent to those of carriers in the corresponding DOX formulation groups, was also added into cells. Cells were incubated for 48 h and cell viability was determined by MTT assay. Briefly, ten microliters of 3-(4, 5-dimethylthiazol-2-yl)-2,5-diphenyltetrazoliumbromide (MTT) (5mg/mL in PBS) were added to cells. Following incubation for 4 h, the medium was removed and MTT formazan was solubilized by DMSO. The absorbance was measured by a microplate reader with wavelength at 590 nm and reference wavelength at 620 nm. Untreated cells were used as a control. Cell viability was calculated as $[(OD_{treat} - OD_{blank})/(OD_{control} - OD_{blank}) \times 100\%]$.

2.2.6 Western blot

Western immunoblotting was conducted with 4T1.2 cells. Cells were treated with 0.1% DMSO (control) or indicated concentrations (1 μM or 5 μM) of SAHA or POEG-*b*-PSAHA, respectively. After 24 h treatment, cells were rinsed twice with ice-cold PBS and lysed by RIPA buffer. The lysates were centrifuged at 12,500 rpm for 10 min. Samples with equal amounts of total cellular proteins were subjected to sodium dodecylsulfate polyacryl amide gel electrophoresis (SDS-PAGE), followed by transferring to nitrocellulose membranes. The membranes were first blocked in 5% nonfat dry milk dissolved in DPBS with 0.1% Tween 20 (PBST) for 1 h at RT, and then incubated with primary antibody at a final dilution of 1:1,000

in 5% BSA in PBST overnight at 4 °C. After washing three times with PBST, the membranes were incubated with secondary antibody at a final dilution of 1:5,000 in PBST for 1 h at room temperature. After washing three times with PBST, bound antibodies were detected by chemiluminescence. Beta-actin was used as the loading control. Primary antibodies for AC-H3 and AC-H4 were from Cell Signaling Technology (MA, USA) and the antibody for beta-actin was from Sigma-Aldrich (MO, USA).

2.2.7 Plasma pharmacokinetics

For plasma pharmacokinetics, DOX/POEG-*b*-PSAHA micelles or free DOX.HCl was injected intravenously into tumor-free female CD1 mice at a DOX dose of 5 mg/kg, with five mice in each group. Blood samples were collected in heparinized tubes at designated time points (3min, 10 min, 30 min, 1 h, 2 h, 4 h, 8 h and 12 h) post injection. The samples were centrifuged at 12,500 rpm for 10 min at 4 °C and 20 μL of the supernatant were collected. Then 200 μL methanol, containing 500 ng/mL daunorubicin as the internal standard, was added and vortexed for 3 min. The samples were centrifuged at 12,500 rpm for 10 min at 4 °C and 150 μL of the clear supernatant was collected and injected into HPLC for DOX analysis.

2.2.8 *In vivo* therapeutic study

The *in vivo* antitumor efficacy of the DOX loaded in POEG-*b*-PSAHA prodrug nanocarrier was tested in a syngeneic 4T1.2 mouse breast cancer model. Female BALB/c mice were s.c. inoculated with 4T1.2 cells at right mammary fat pad with 2×10^5 cells/mouse. When the tumor sizes reached around 50 mm^3, mice were randomly divided into five groups (n=5), and treated via tail vein injection with PBS, DOX.HCl, Doxil, DOX/POEG-*b*-POM or DOX/POEG-*b*-PSAHA micelles at a DOX dose of 5 mg/kg on days 1, 4 and 7, respectively.

Tumor sizes were measured with the digital caliper every three days following the initiation of the treatment and calculated by the formula: $(L\times W^2)/2$, in which L is the longest and W is the shortest in tumor diameters (mm). Data were plotted as the actual tumor volume. Body weights were also monitored for the indication of toxicity. On day 23 post injection, all mice were sacrificed and tumor tissues were collected for measurement of weights and photography.

2.2.8 Statistical analysis

In vitro or *in vivo* data are presented as mean ± standard deviation (SD) or mean ± standard error of mean (SEM), respectively. Statistical analysis was performed with two-tailed Student's T test or one-way analysis of variance (ANOVA) for two groups or multiple groups, respectively, followed by Turkey simultaneous post hoc test. In all statistical analyses, $P < 0.05$ was considered statistically significant.

3. Results and Discussion:

3.1 Effect of combination of SAHA and DOX on tumor cell proliferation

The proliferation inhibitory effect of SAHA and DOX was examined in 4T1.2 and HCT-116 cell lines. As shown in Fig. 1A, SAHA or DOX inhibited the proliferation of 4T1.2 cells in a concentration-dependent manner. It was also apparent that combination of the two agents led to enhanced cytotoxicity. A similar combinational effect was found in HCT-116 cells (Fig. 1B). Combination index (CI) was then calculated to assess a potential synergism between SAHA and DOX, by the equation $CI=(d1/IC_{50}1)+ (d2/IC_{50}2)$, with d1 or d2 being the concentration of SAHA or DOX required to achieve 50% killing effect in co-treatment, while $IC_{50}1$ or $IC_{50}2$ being IC50 of SAHA or DOX in single treatment, respectively. The CI of

SAHA and DOX combination were 0.67 and 0.84 in 4T1.2 and HCT-116 cells respectively, suggesting a synergism between the two drugs.

3.2 Synthesis and characterization of the POEG-*b*-PSAHA polymer

We initially designed and synthesized a SAHA-based monomer by directly conjugating SAHA with methacryloyl chloride. The macro-chain transfer agent POEG was then synthesized by RAFT polymerization of hydrophilic OEGMA monomer, which was further used to initiate the polymerization of hydrophobic SAHA monomer. However, micelles formed from this polymer had a size around 160 nm (data not shown), which is suboptimal for EPR effect. In order to decrease the hydrodynamic size, we re-designed a new SAHA monomer by introducing an additional 4 carbon hydrophobic chain and another benzyl ring to SAHA (Scheme. 1). Vinylbenzyl chloride was linked to succinic acid, followed by the condensation reaction with SAHA to form a hydrolysable diester bond. Then RAFT polymerization was similarly performed as described above, yielding the amphiphilic POEG-*b*-PSAHA block copolymer. The structure of POEG-*b*-PSAHA polymer was confirmed by ^{1}H NMR (Fig. 2), and the average degree of polymerization of the SAHA monomer was calculated. Each POEG-*b*-PSAHA molecule contained 12 units of SAHA.

3.3 Characterizations of DOX-loaded POEG-*b*-PSAHA micelles

Blank or DOX-loaded POEG-*b*-PSAHA micelles were prepared by a simple film hydration method. Unlike the initial SAHA polymer that formed relatively large-sized micelles (~160 nm), the size of drug-free POEG-*b*-PSAHA micelles was significantly smaller (63.7 nm). This is likely due to more effective carrier-carrier interaction as a result of incorporation of additional 4 carbon hydrophobic chain and another benzyl ring to SAHA monomer. Loading of DOX into POEG-*b*-PSAHA micelles at a carrier/drug weight ratio of 20:1 only led to a

slight increase in the particle size (~70 nm) (Fig. 3B). TEM showed sphere shape with a uniform size distribution, which was consistent with DLS (Fig. 3C, D). The size, DLC, and formulation stability of drug-loaded POEG-*b*-PSAHA micelles were then examined and listed in Table 1. DOX could be loaded into POEG-*b*-PSAHA micelles at a carrier/drug ratio as low as 5/1 (mg/mg), at which ratio DOX loading capacity was 14.9 % and DOX-loaded micelles were stable for 5 days at 4 °C. With an increase in the carrier/drug ratio, the drug encapsulation efficiency and colloidal stability were further improved. As shown in Table 1, at a carrier/drug ratio of 50:1, DOX-loaded micelles were stable for 50 days at 4 °C. A carrier/drug mass ratio of 20:1 and 5:1 was used for *in vitro* and *in vivo* study, respectively.

Fig. 4 shows that the CMC of POEG-*b*-PSAHA micelles was around 0.004 mg/mL as determined by a rapid change of fluorescence intensity of loaded nile red probe during serial dilution. This low CMC of POEG-*b*-PSAHA shall provide a good stability for the micelles upon dilution in blood stream after i.v. injection.

3.4 *In vitro* drug release

The release profile of DOX loaded in POEG-*b*-PSAHA micelles in PBS was investigated by a dialysis method and compared to that of free DOX. As shown in Fig. 5, around 50% of DOX was released from DOX.HCl in the first two hours and 85% of total DOX was released within 12 h. In contrast, less than 1% of DOX was released from the DOX-loaded POEG-*b*-PSAHA micelles in the first hour and a relatively sustained release continued for 72 hours, with only around 30% of total drug released. The slow release kinetics might be due to strong carrier-drug interaction, including hydrophobic interaction and π-π stacking, which shall provide a good stability of DOX/POEG-*b*-PSAHA in blood stream.

3.5 *In vitro* cytotoxicity of drug-free or DOX-loaded POEG-*b*-PSAHA micelles

To evaluate whether POEG-*b*-PSAHA prodrug micelles maintained the ability of SAHA to inhibit tumor cell proliferation, 4T1.2, MCF-7 or HCT-116 cells were treated with POEG-*b*-PSAHA micelles or free SAHA (in DMSO) for 48 h. As shown in Fig. 6A, free SAHA inhibited the proliferation of 4T1.2 tumor cells in a dose-dependent manner, while POEG-*b*-PSAHA showed a comparable cytotoxicity. Similar results were shown in MCF-7 and HCT-116 tumor cells (Fig. 6B & C), suggesting that SAHA could be effectively released from POEG-*b*-PSAHA via the cleavage of carbamide bond.

The *in vitro* cytotoxicity of DOX-loaded POEG-*b*-PSAHA micelles was also tested, in comparison with DOX.HCl and DOX loaded in pharmacologically "inert" POEG-*b*-POM micelles. POEG-*b*-PSAHA and POEG-*b*-POM carrier alone were included as controls and were used at the same concentrations as those used in drug-loaded micelles. As shown in Fig. 7A, POEG-*b*-POM blank micelles showed minimal cytotoxicity even at the highest concentration (20 μg/mL). In contrast, blank POEG-*b*-PSAHA micelles exhibited significant cytotoxicity, which was comparable to that of DOX.HCl. DOX loaded in POEG-*b*-PSAHA was more potent in killing tumor cells than DOX.HCl and DOX/POEG-*b*-POM formulation. Similar results were observed in MCF-7 and HCT-116 cells (Fig. 7B & C). It is likely that the improved cytotoxicity of DOX/POEG-*b*-PSAHA is attributed to a synergistic action between DOX and SAHA that was released from the carrier following intracellular delivery.

3.6 Effect of POEG-*b*-PSAHA on histone acetylation

To investigate if the POEG-*b*-PSAHA-mediated cytotoxicity is attributed to the specific action of released SAHA, we examined the efficiency of POEG-*b*-PSAHA in modulating the acetylation of histone in 4T1.2 breast cancer cells by Western blot. As shown in Fig. 8, the basal levels of acetylated H3 and H4 were very low. SAHA treatment at submicromolar

concentrations for 24 h led to significant increases in their levels in a dose-dependent manner. Interestingly, POEG-*b*-PSAHA was comparable to or even more potent than free SAHA in inducing acetylation of H3 or H4 at the same concentrations of SAHA. These data indicated that POEG-*b*-PSAHA well retained the bioactivity of SAHA in inhibiting HDAC, resulting in the hyperacetylation of histone H3 and H4 and subsequently inhibition of cancer cell proliferation. The possible mechanism for the comparable or even further enhanced efficacy in histone acetylation is that POEG-*b*-PSAHA protected the hydroxamic acid of SAHA from hydrolysis and pharmacologically active SAHA was slowly released from the polymer over a prolonged period of time. On the other hand, free SAHA with unprotected hydroxamic acid may be subjected to rapid metabolic conversion to inactive metabolites, SAHA-glucuronide and 4-anilino-4-oxobutanoic acid (Hattori et al., 2011).

3.7 Plasma pharmacokinetics

The DOX/POEG-*b*-PSAHA or DOX.HCl was injected into tumor-free mice at a DOX dose of 5 mg/kg. The plasma concentrations of DOX were examined at different time points. The initial concentration of POEG-*b*-PSAHA was around 1 mg/mL, which was 250-fold higher than its CMC (0.004 mg/mL). The concentrations of DOX in the blood following i.v. injection of different treatments as a function of time were illustrated in Fig. 9. Compared to DOX.HCl group, the plasma concentrations of DOX from the group treated with POEG-*b*-PSAHA/DOX were significantly higher at early time points and maintained at relatively high levels until 12 h, which is likely attributed to the surface modification of PEG and stealth-shielding against RES system. These data demonstrated that DOX formulated in POEG-*b*-PSAHA prodrug micelles was able to circulate for a significantly longer period of time in the blood.

3.8 *In vivo* therapeutic study

Following the demonstration of a potential synergistic effect between POEG-*b*-PSAHA-based carrier and the co-delivered DOX in cultured cancer cells, we then evaluated the tumor growth inhibitory effect of DOX/POEG-*b*-PSAHA in a highly metastatic syngeneic murine breast cancer model (4T1.2, s.c.). As shown in Fig. 10A, free DOX exhibited a modest antitumor activity at a dose of 5 mg/kg. Doxil and DOX/POEG-*b*-POM formulations were more effective than free DOX. At the same dose of DOX, DOX/POEG-*b*-PSAHA was most effective in inhibiting the tumor growth (Fig. 10A). Fig. 10 B & D show the weights and images of tumor tissues collected at the end of the experiment, which were consistent with the result of tumor growth curves (Fig. 10A). The significantly improved anti-tumor activity of DOX/POEG-*b*-PSAHA is likely attributed to the effective accumulation of the nanocarrier at tumor sites due to its small size (~70 nm). The synergistic effect between the released SAHA and co-delivered DOX may also play an important role in tumor inhibition. More studies are needed in the future to further delineate the underlying mechanism. There were slight increases in body weights in all groups over the period of study, suggesting the negligible toxicity of DOX/POEG-*b*-PSAHA micelles in vivo.

4. Conclusion:

We have developed a well-characterized POEG-*b*-PSAHA prodrug micellar nanocarrier, which consists of a hydrophobic segment composed of 12 SAHA-based units, and a POEG hydrophilic segment for efficient entrapment of DOX. Our POEG-*b*-PSAHA prodrug micelles well retained the biological activity of SAHA in inhibiting the proliferation of tumor cells and promoting the acetylation of histone H3 and H4. Besides, POEG-*b*-PSAHA was effective in formulating DOX and demonstrated a slow kinetics of drug release. More

importantly, *in vivo* delivery of DOX via POEG-*b*-PSAHA led to significant inhibition of 4T1.2 tumor, much more effectively than DOX.HCl, Doxil and DOX/POEG-*b*-POM.

Acknowledgments

We would like to thank Dr. Ming Sun for her help with negative EM study.

Declaration of interest

This work was supported by NIH grants no. R01CA174305 and no. R01CA219399. The authors declare no competing financial interest.

Reference:

ARNOLD, N. B., ARKUS, N., GUNN, J. & KORC, M. 2007. The Histone Deacetylase Inhibitor Suberoylanilide Hydroxamic Acid Induces Growth Inhibition and Enhances Gemcitabine-Induced Cell Death in Pancreatic Cancer. *Clinical Cancer Research,* 13**,** 18-26.

AVENDAÑO, C. & MENÉNDEZ, J. C. 2015. Chapter 8 - Epigenetic Therapy of Cancer. *Medicinal Chemistry of Anticancer Drugs (Second Edition).* Boston: Elsevier.

BERGER, S. L., KOUZARIDES, T., SHIEKHATTAR, R. & SHILATIFARD, A. 2009. An operational definition of epigenetics. *Genes Dev,* 23**,** 781-3.

BUTLER, L. M., AGUS, D. B., SCHER, H. I., HIGGINS, B., ROSE, A., CORDON-CARDO, C., THALER, H. T., RIFKIND, R. A., MARKS, P. A. & RICHON, V. M. 2000. Suberoylanilide hydroxamic acid, an inhibitor of histone deacetylase, suppresses the growth of prostate cancer cells in vitro and in vivo. *Cancer Res,* 60**,** 5165-70.

CAMERON, E. E., BACHMAN, K. E., MYOHANEN, S., HERMAN, J. G. & BAYLIN, S. B. 1999. Synergy of demethylation and histone deacetylase inhibition in the re-expression of genes silenced in cancer. *Nat Genet,* 21**,** 103-7.

CHEN, C. S., WANG, Y. C., YANG, H. C., HUANG, P. H., KULP, S. K., YANG, C. C., LU, Y. S., MATSUYAMA, S., CHEN, C. Y. & CHEN, C. S. 2007. Histone deacetylase inhibitors sensitize prostate cancer cells to agents that produce DNA double-strand breaks by targeting Ku70 acetylation. *Cancer Res,* 67**,** 5318-27.

CHUNG, Y.-M., EL-SHAZLY, M., CHUANG, D.-W., HWANG, T.-L., ASAI, T., OSHIMA, Y., ASHOUR, M. L., WU, Y.-C. & CHANG, F.-R. 2013. Suberoylanilide Hydroxamic Acid, a Histone Deacetylase Inhibitor, Induces the Production of Anti-inflammatory Cyclodepsipeptides from Beauveria felina. *Journal of Natural Products,* 76**,** 1260-1266.

COHEN, L. A., AMIN, S., MARKS, P. A., RIFKIND, R. A., DESAI, D. & RICHON, V. M. 1999. Chemoprevention of carcinogen-induced mammary tumorigenesis by the hybrid polar cytodifferentiation agent, suberanilohydroxamic acid (SAHA). *Anticancer Res,* 19**,** 4999-5005.

CROY, S. R. & KWON, G. S. 2006. Polymeric micelles for drug delivery. *Curr Pharm Des,* 12**,** 4669-84.

DESAI, D., DAS, A., COHEN, L., EL-BAYOUMY, K. & AMIN, S. 2003. Chemopreventive efficacy of suberoylanilide hydroxamic acid (SAHA) against 4-(methylnitrosamino)-1-(3-pyridyl)-1-butanone (NNK)-induced lung tumorigenesis in female A/J mice. *Anticancer Res,* 23**,** 499-503.

DOWDY, S. C., JIANG, S., ZHOU, X. C., HOU, X., JIN, F., PODRATZ, K. C. & JIANG, S.-W. 2006. Histone deacetylase inhibitors and paclitaxel cause synergistic effects on apoptosis and microtubule stabilization in papillary serous endometrial cancer cells. *Molecular Cancer Therapeutics,* 5**,** 2767-2776.

EYUPOGLU, I. Y., HAHNEN, E., BUSLEI, R., SIEBZEHNRUBL, F. A., SAVASKAN, N. E., LUDERS, M., TRANKLE, C., WICK, W., WELLER, M., FAHLBUSCH, R. & BLUMCKE, I. 2005. Suberoylanilide hydroxamic acid (SAHA) has potent anti-glioma properties in vitro, ex vivo and in vivo. *J Neurochem,* 93**,** 992-9.

FALKENBERG, K. J. & JOHNSTONE, R. W. 2014. Histone deacetylases and their inhibitors in cancer, neurological diseases and immune disorders. *Nat Rev Drug Discov,* 13**,** 673-91.

FUINO, L., BALI, P., WITTMANN, S., DONAPATY, S., GUO, F., YAMAGUCHI, H., WANG, H. G., ATADJA, P. & BHALLA, K. 2003. Histone deacetylase inhibitor LAQ824 down-regulates Her-2 and sensitizes human breast cancer cells to trastuzumab, taxotere, gemcitabine, and epothilone B. *Mol Cancer Ther,* 2**,** 971-84.

GIBNEY, E. R. & NOLAN, C. M. 2010. Epigenetics and gene expression. *Heredity,* 105**,** 4-13.

GREGORY, P. D., WAGNER, K. & HORZ, W. 2001. Histone acetylation and chromatin remodeling. *Exp Cell Res,* 265**,** 195-202.

GRUNSTEIN, M. 1997. Histone acetylation in chromatin structure and transcription. *Nature,* 389**,** 349-52.

HALKIDOU, K., GAUGHAN, L., COOK, S., LEUNG, H. Y., NEAL, D. E. & ROBSON, C. N. 2004. Upregulation and nuclear recruitment of HDAC1 in hormone refractory prostate cancer. *Prostate,* 59**,** 177-89.

HATTORI, Y., NAGAOKA, Y., KUBO, M., YAMASAKU, H., ISHII, Y., OKITA, H., NAKANO, H., UESATO, S. & MAITANI, Y. 2011. Antitumor effect of liposomal histone deacetylase inhibitor-lipid conjugates in vitro. *Chem Pharm Bull (Tokyo),* 59**,** 1386-92.

HE, L. Z., TOLENTINO, T., GRAYSON, P., ZHONG, S., WARRELL, R. P., JR., RIFKIND, R. A., MARKS, P. A., RICHON, V. M. & PANDOLFI, P. P. 2001. Histone deacetylase inhibitors induce remission in transgenic models of therapy-resistant acute promyelocytic leukemia. *J Clin Invest,* 108**,** 1321-30.

JOHNSTONE, R. W. 2002. Histone-deacetylase inhibitors: novel drugs for the treatment of cancer. *Nat Rev Drug Discov,* 1**,** 287-99.

KIM, M. S., BLAKE, M., BAEK, J. H., KOHLHAGEN, G., POMMIER, Y. & CARRIER, F. 2003. Inhibition of histone deacetylase increases cytotoxicity to anticancer drugs targeting DNA. *Cancer Res,* 63**,** 7291-300.

KOUZARIDES, T. 2007. Chromatin Modifications and Their Function. *Cell,* 128**,** 693-705.

LEE, J. H. & NAN, A. 2012. Combination drug delivery approaches in metastatic breast cancer. *Journal of drug delivery,* 2012.

MARCHION, D. C., BICAKU, E., DAUD, A. I., SULLIVAN, D. M. & MUNSTER, P. N. 2005a. In vivo synergy between topoisomerase II and histone deacetylase inhibitors: predictive correlates. *Mol Cancer Ther,* 4**,** 1993-2000.

MARCHION, D. C., BICAKU, E., TURNER, J. G., DAUD, A. I., SULLIVAN, D. M. & MUNSTER, P. N. 2005b. Synergistic interaction between histone deacetylase and topoisomerase II inhibitors is mediated through topoisomerase IIbeta. *Clin Cancer Res,* 11**,** 8467-75.

MARKS, P., RIFKIND, R. A., RICHON, V. M., BRESLOW, R., MILLER, T. & KELLY, W. K. 2001. Histone deacetylases and cancer: causes and therapies. *Nat Rev Cancer,* 1**,** 194-202.

MARKS, P. A. 2007. Discovery and development of SAHA as an anticancer agent. *Oncogene,* 26**,** 1351-6.

MARKS, P. A. & BRESLOW, R. 2007. Dimethyl sulfoxide to vorinostat: development of this histone deacetylase inhibitor as an anticancer drug. *Nat Biotechnol,* 25**,** 84-90.

MOHAMED, E. A., ZHAO, Y., MESHALI, M. M., REMSBERG, C. M., BORG, T. M., FODA, A. M., TAKEMOTO, J. K., SAYRE, C. L., MARTINEZ, S. E., DAVIES, N. M. & FORREST, M. L. 2012. Vorinostat with sustained exposure and high solubility in poly(ethylene glycol)-b-poly(DL-lactic acid) micelle nanocarriers: characterization and effects on pharmacokinetics in rat serum and urine. *J Pharm Sci,* 101**,** 3787-98.

MUNSTER, P. N., MARCHION, D., THOMAS, S., EGORIN, M., MINTON, S., SPRINGETT, G., LEE, J. H., SIMON, G., CHIAPPORI, A., SULLIVAN, D. & DAUD, A. 2009. Phase I trial of vorinostat and doxorubicin in solid tumours: histone deacetylase 2 expression as a predictive marker. *British Journal of Cancer,* 101**,** 1044-1050.

NIMMANAPALLI, R., FUINO, L., STOBAUGH, C., RICHON, V. & BHALLA, K. 2003. Cotreatment with the histone deacetylase inhibitor suberoylanilide hydroxamic acid (SAHA) enhances imatinib-induced apoptosis of Bcr-Abl–positive human acute leukemia cells. *Blood,* 101**,** 3236-3239.

PARHI, P., MOHANTY, C. & SAHOO, S. K. 2012. Nanotechnology-based combinational drug delivery: an emerging approach for cancer therapy. *Drug Discovery Today,* 17**,** 1044-1052.

RIKIISHI, H., SHINOHARA, F., SATO, T., SATO, Y., SUZUKI, M. & ECHIGO, S. 2007. Chemosensitization of oral squamous cell carcinoma cells to cisplatin by histone deacetylase inhibitor, suberoylanilide hydroxamic acid. *Int J Oncol,* 30**,** 1181-8.

SONG, J., NOH, J. H., LEE, J. H., EUN, J. W., AHN, Y. M., KIM, S. Y., LEE, S. H., PARK, W. S., YOO, N. J., LEE, J. Y. & NAM, S. W. 2005. Increased expression of histone deacetylase 2 is found in human gastric cancer. *APMIS,* 113**,** 264-8.

SUN, J., CHEN, Y., LI, K., HUANG, Y., FU, X., ZHANG, X., ZHAO, W., WEI, Y., XU, L., ZHANG, P., VENKATARAMANAN, R. & LI, S. 2016. A prodrug micellar carrier assembled from polymers with pendant farnesyl thiosalicylic acid moieties for improved delivery of paclitaxel. *Acta Biomater,* 43**,** 282-91.

THORN, C. F., OSHIRO, C., MARSH, S., HERNANDEZ-BOUSSARD, T., MCLEOD, H., KLEIN, T. E. & ALTMAN, R. B. 2011. Doxorubicin pathways: pharmacodynamics and adverse effects. *Pharmacogenet Genomics,* 21**,** 440-6.

THURN, K. T., THOMAS, S., MOORE, A. & MUNSTER, P. N. 2011. Rational therapeutic combinations with histone deacetylase inhibitors for the treatment of cancer. *Future oncology (London, England),* 7**,** 263-283.

ZHANG, X., HUANG, Y., ZHAO, W., LIU, H., MARQUEZ, R., LU, J., ZHANG, P., ZHANG, Y., LI, J., GAO, X., VENKATARAMANAN, R., XU, L. & LI, S. 2014a. Targeted delivery of anticancer agents via a dual function nanocarrier with an interfacial drug-interactive motif. *Biomacromolecules,* 15**,** 4326-35.

ZHANG, X., LIU, K., HUANG, Y., XU, J., LI, J., MA, X. & LI, S. 2014b. Reduction-sensitive dual functional nanomicelles for improved delivery of paclitaxel. *Bioconjug Chem,* 25**,** 1689-96.

ZHU, P., MARTIN, E., MENGWASSER, J., SCHLAG, P., JANSSEN, K. P. & GOTTLICHER, M. 2004. Induction of HDAC2 expression upon loss of APC in colorectal tumorigenesis. *Cancer Cell,* 5**,** 455-63.

Fig. 1

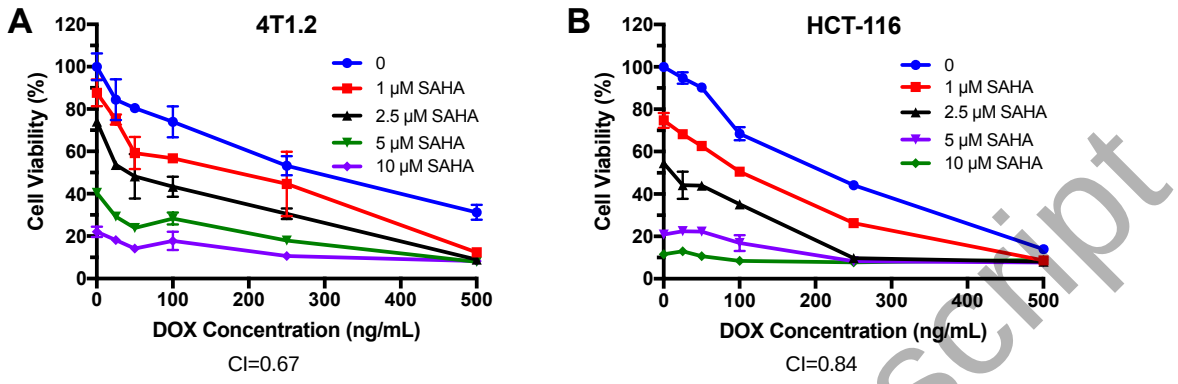

Fig. 2

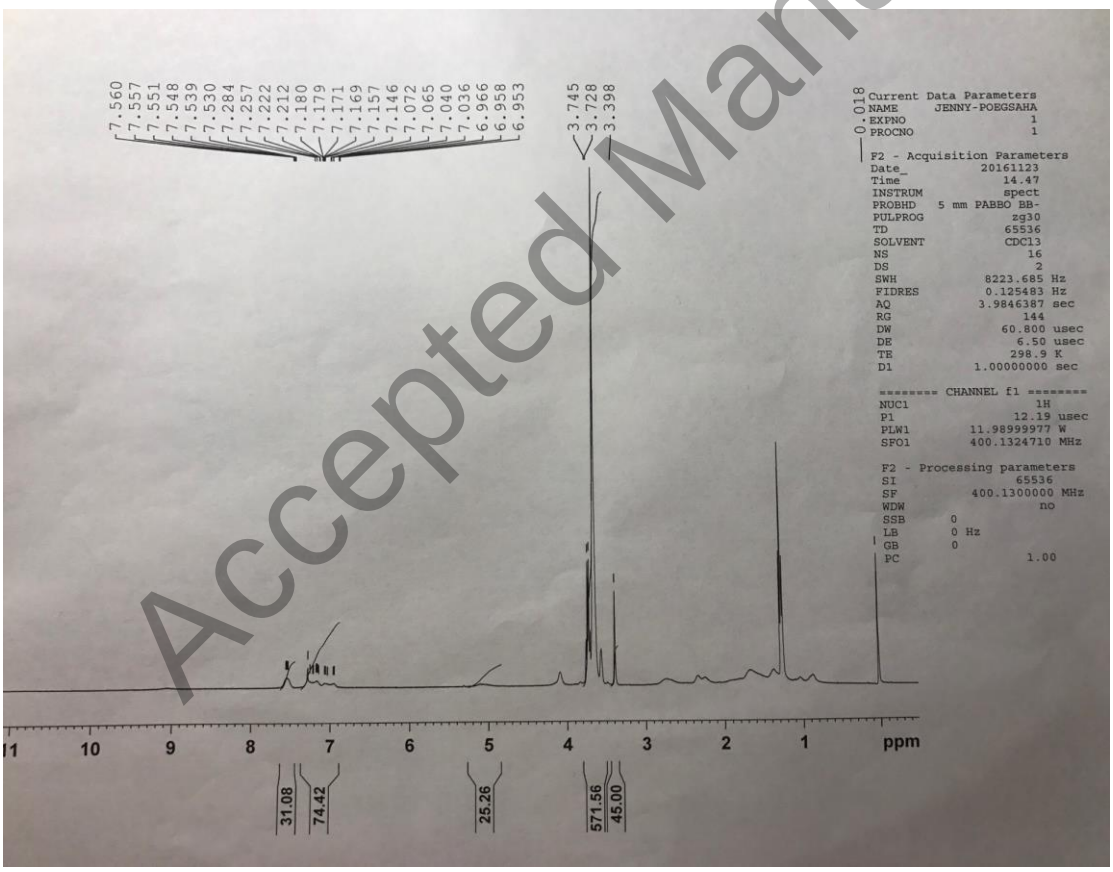

Fig. 3

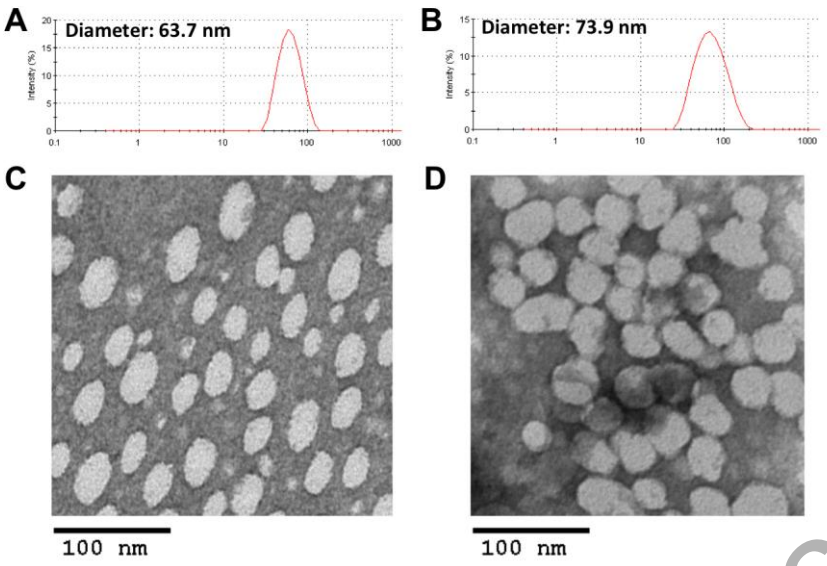

Fig. 4

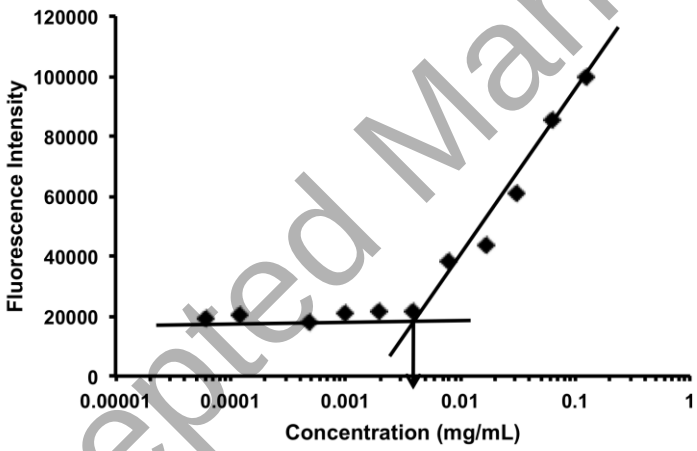

Fig. 5

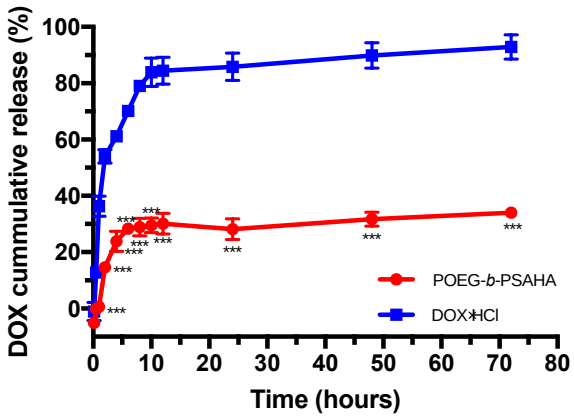

Fig. 6

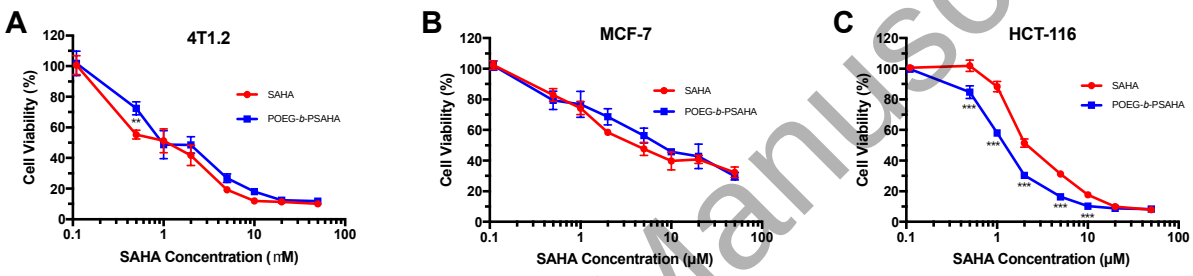

Fig. 7

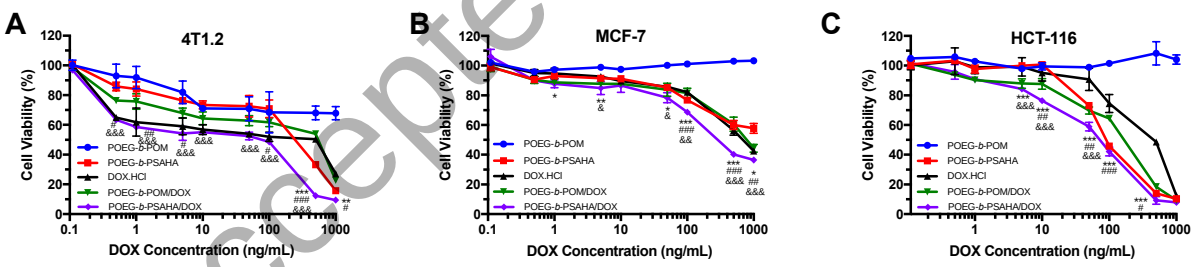

Fig. 8

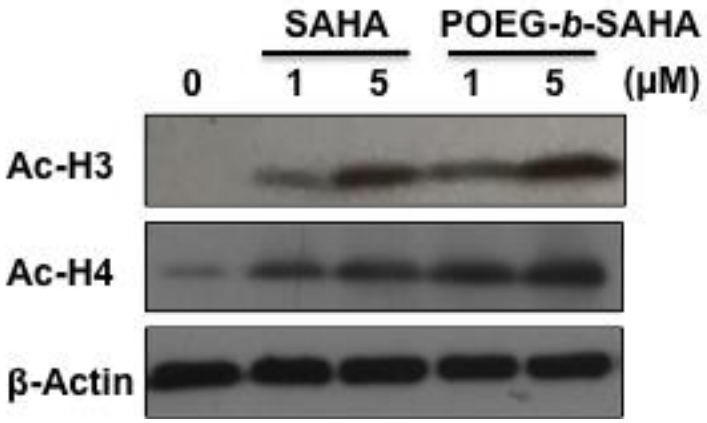

Fig. 9

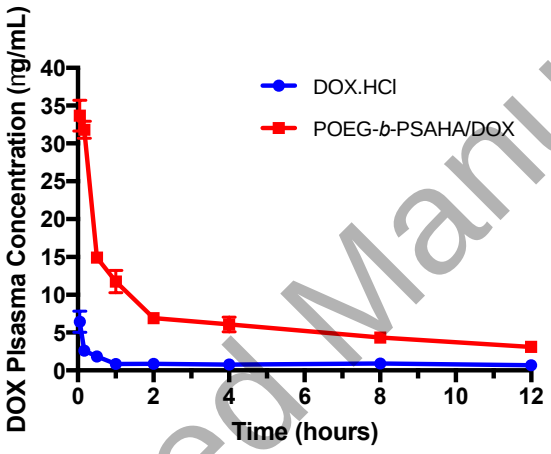

Fig. 10

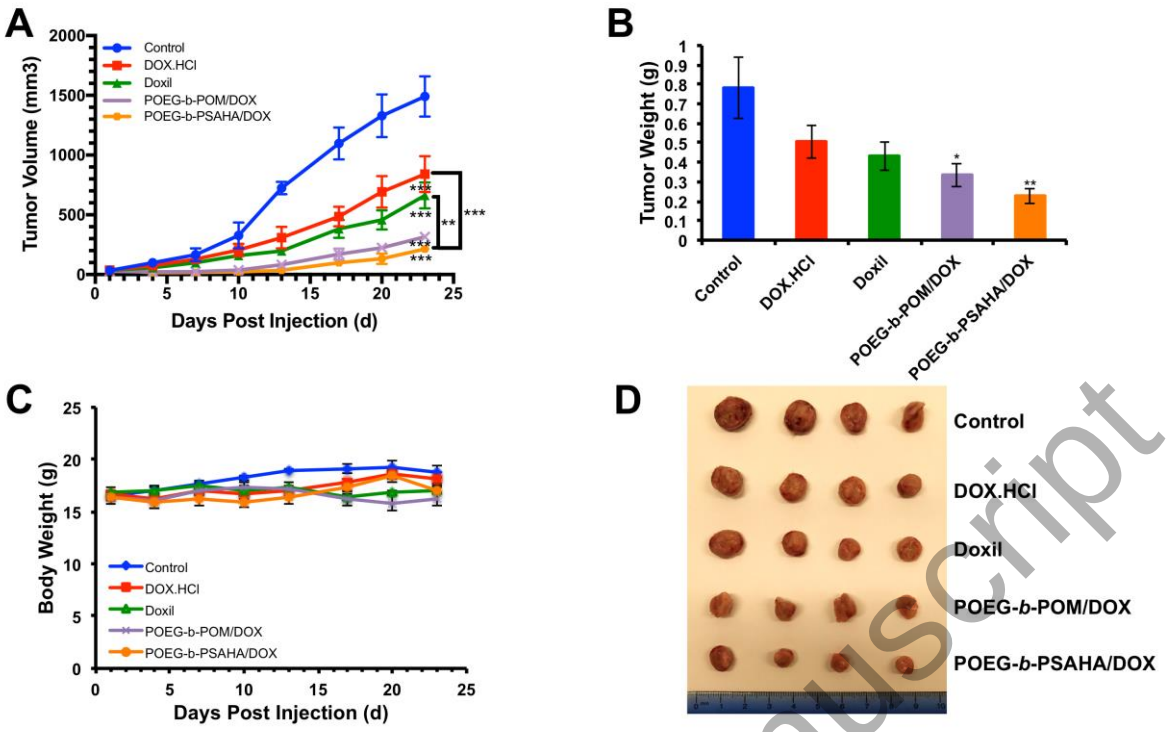

Fig. 11

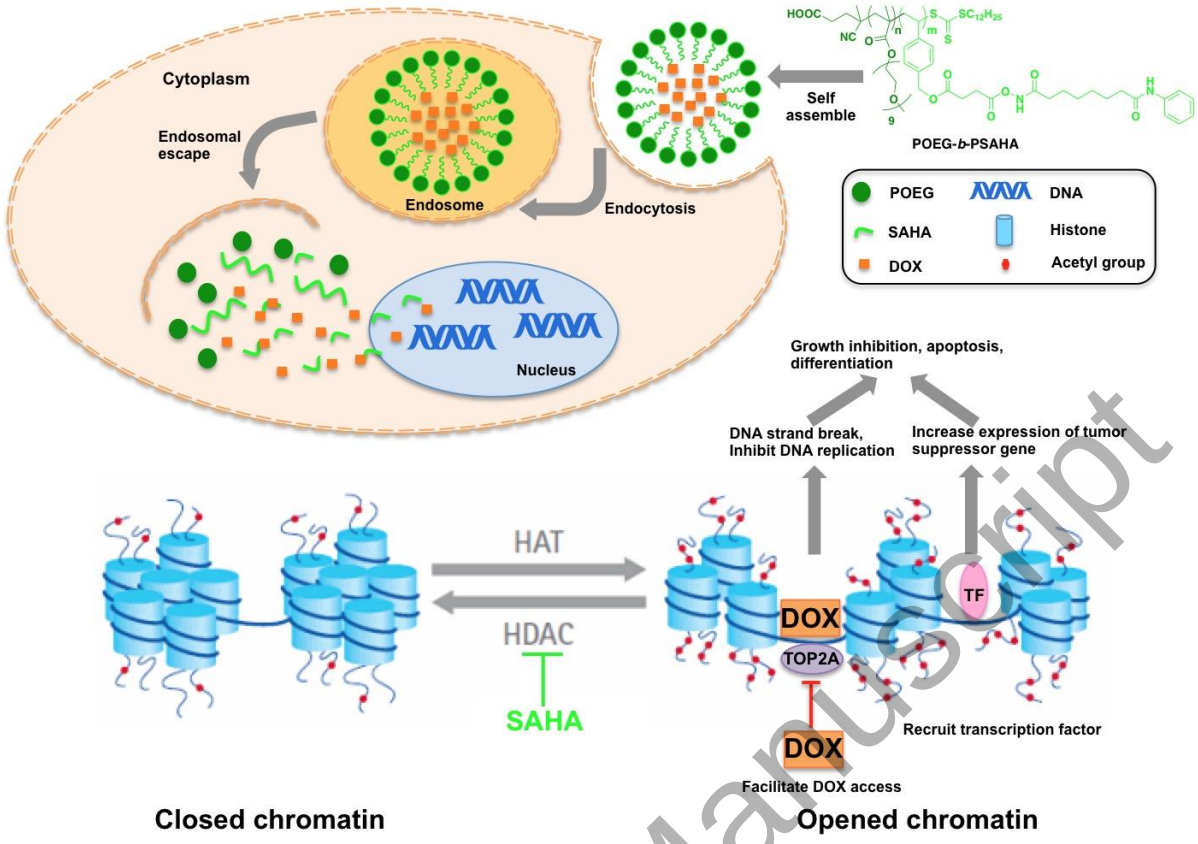

Scheme 1.

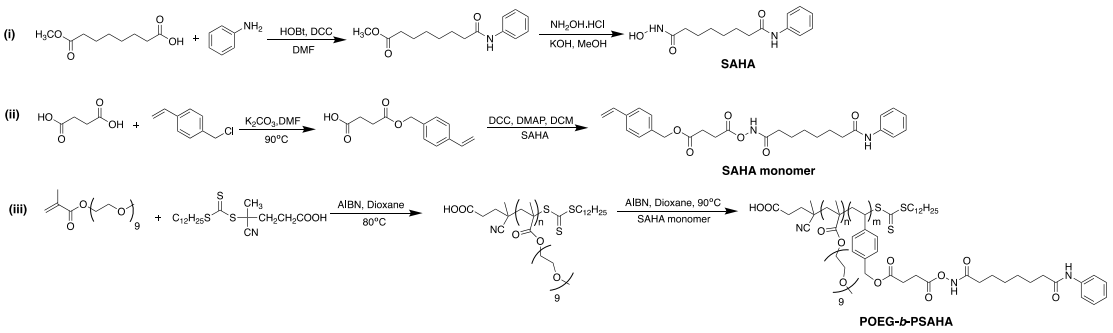

Table 1.

Micelles	Mass ratio (mg: mg) [a]	Size (nm)[b]	PDI[c]	DLC(%)[d]	DLE(%)[e]	Stability[f]
POEG-*b*-PSAHA:		63.7 ± 0.7	0.14 ± 0.01			
POEG-*b*-PSAHA: DOX	5:1	78.4 ± 0.4	0.22 ± 0.01	14.9	89.3	5 d
POEG-*b*-PSAHA: DOX	10: 1	75.9 ± 0.6	0.18 ± 0.01	8.2	90.6	9 d
POEG-*b*-PSAHA: DOX	20:1	73.9 ± 0.9	0.26 ± 0.01	4.5	93.5	17 d
POEG-*b*-PSAHA: DOX	30: 1	79.7 ± 0.3	0.23 ± 0.01	3.0	92.3	32 d
POEG-*b*-PSAHA: DOX	50:1	86.6 ± 0.2	0.20± 0.01	1.9	96.7	50 d

[a)] DOX concentration in micelles was kept at 0.5 mg/mL. [b)] Measured by dynamic light scattering particle sizer. [c)] PDI = polydispersity index. [d)] DLC = drug loading capacity. [e)] DLE = drug loading efficiency. f) Data mean there was no noticeable size change and visible precipitates during the follow-up period at 4 °C.

Figure legend:

Fig. 1. Synergistic effect between SAHA and DOX in inhibiting the proliferation of tumor cells. 4T1.2 (A) or HCT-116 (B) cells were treated with various concentrations of free SAHA, free DOX or the combination of SAHA and DOX. After 48 h, the cytotoxicity was determined by MTT assay. The experiments was performed in triplicate and repeated three times. Data are presented as means ± SD.

Fig. 2. ^{1}H NMR spectra of POEG-*b*-PSAHA polymer in $CDCl_3$.

Fig. 3. Particle size distribution of blank POEG-*b*-PSAHA micelles (A) and DOX-loaded POEG-*b*-PSAHA micelles (B). TEM images of blank POEG-*b*-PSAHA micelles (C) and DOX-loaded POEG-*b*-PSAHA micelles (D). Scale bar is 100 nm.

Fig. 4. CMC of POEG-*b*-PSAHA micelles using nile red as a fluorescence probe. The fluorescence intensity of nile red was collected at the emission wavelength of 647 nm and the excitation wavelength of 550 nm. The fluorescence intensity was plotted versus concentrations of POEG-*b*-PSAHA copolymer. Values reported are the means ± SD for triplicate samples.

Fig. 5. Cumulative DOX release profile from POEG-*b*-PSAHA micelles with free DOX as a control. PBS was used as the release medium. DOX concentration was fixed at 0.5 mg/mL. Values reported are the means ± SD for triplicate samples. *** $P < 0.001$ (POEG-*b*-PSAHA/DOX vs. free DOX).

Fig. 6. MTT cytotoxicity of POEG-*b*-PSAHA prodrug micelles in 4T1.2 mouse breast cancer cell line (A), MCF-7 human breast cancer cell line (B), and HCT-116 human colon cancer cell line (C) in comparison to free SAHA. Cells were treated for 48 h and values reported are the means ± SD for triplicate samples. **$P < 0.01$, ***$P<0.01$ (POEG-*b*-PSAHA vs. SAHA).

Fig. 7. MTT cytotoxicity assay of DOX-loaded POEG-*b*-PSAHA micelles in 4T1.2 (A), MCF-7 (B) and HCT-116 (C) tumor cells after 48 h treatment. Data are presented as the means ± SD for triplicate samples. *P<0.05, **P<0.01, ***P<0.001 (POEG-*b*-PSAHA/DOX vs. DOX.HCl); $^{\#}$P< 0.05, $^{\#\#}$P<0.01, $^{\#\#\#}$P<0.001 (POEG-*b*-PSAHA/DOX vs. POEG-*b*-POM/DOX); $^{\&}$P < 0.05, $^{\&\&}$P<0.01, $^{\&\&\&}$P<0.001 (POEG-*b*-PSAHA/DOX vs. POEG-*b*-PSAHA).

Fig. 8. Effect of POEG-*b*-PSAHA prodrug micelles on expression of acetylated histone 3 (Ac-H3) and acetylated histone 4 (Ac-H4) compared to free SAHA. 4T1.2 cells were treated with various concentrations of SAHA or POEG-*b*-PSAHA at an equivalent concentration of SAHA for 24 h. Western blotting was performed with total protein extracts using antibodies against acetylated H3 and H4. Equal loading and transfer were verified by reproving the membranes for β-actin.

Fig. 9. Plasma pharmacokinetics of DOX.HCl and DOX/POEG-*b*-PSAHA micelles in tumor-free female CD1 mice at the same dose of 5 mg DOX/kg. Values reported are the means ± SEM, n =5.

Fig. 10. (A) Antitumor activity of DOX.HCl, Doxil, DOX-loaded POEG-*b*-POM and DOX-loaded POEG-*b*-PSAHA micelles in female BALB/c mice bearing 4T1.2 breast tumor. Three injections were given on days 1, 4, 7 and each point represents the mean of actual tumor volume. (B) Weights of tumors collected from different groups at the end of experiment. (C) Changes of body weight in mice receiving different treatments. (D) Photographs of tumors collected from different treatment groups at the end of experiment. Values reported are the means ± SEM, n = 5. *P < 0.05, **P < 0.01, ***P < 0.001 (vs. control).

Fig. 11. The potential mechanism for the synergistic action between DOX and SAHA in tumor cells following the intracellular delivery of DOX/POEG-*b*-PSAHA system.

Scheme 1. Synthesis of the SAHA-monomer and POEG-*b*-PSAHA polymers via RAFT polymerization.

Table 1. Physicochemical characterizations of DOX-loaded POEG-*b*-PSAHA micelles. [a)] DOX concentration in micelles was kept at 0.5 mg/mL. [b)] Measured by dynamic light scattering particle sizer. [c)] PDI = polydispersity index. [d)] DLC = drug loading capacity. [e)] DLE = drug loading efficiency. f) Data mean there was no noticeable size change and visible precipitates during the follow-up period at 4 °C.